JOURNAL OF SOLID STATE CHEMISTRY 66, 263–282 (1987)

Core Projection Effects in Near-Ab-Initio Valence Calculations

II. Ground State Geometry of Octahedral Chromium (I, II, III, and IV) Hexafluorides

V. LUAÑA, G. FERNÁNDEZ RODRIGO, E. FRANCISCO, AND L. PUEYO

Departamento de Química Física, Facultad de Química, Universidad de Oviedo, 33007 Oviedo, Spain

AND M. BERMEJO

Departamento de Física, E.T.S. de Ingenieros de Minas, Universidad de Oviedo, 33004 Oviedo, Spain

Received April 28, 1986; in revised form June 17, 1986

Cluster-*in-vacuo* calculations are reported for the CrF_b^{n-} (n = 2–5) systems at several metal–ligand distances, following the methodology of J. W. Richardson, T. F. Soules, D. M. Vaught, and R. R. Powell (*Phys. Rev. B* **4**, 1721 (1971)) augmented with core-projection operators. The effects of this projection on the computed ground state nuclear potential and the equilibrium geometry have been evaluated. The influence of the type and size of the valence set in the prediction of the geometry of the cluster has also been analyzed. It is found that in the projected calculations such influence is rather small, so that a reliable theoretical prediction can be obtained. The calculations are compared with an extensive collection of experimentally determined geometries. This comparison shows that, in the worst cases, the predicted R_e's and $\bar{\nu}(a_{1g})$'s deviate 0.1–0.2 Å and 100–150 cm^{-1}, respectively, from the experimental values.

I. Introduction

Many properties of a metallic cation M in an ionic lattice can be interpreted in terms of the electronic structure of the cluster MX_n, formed by the cation and its n nearest neighbor anions. The equilibrium metal–ligand distance $R(M - X) = R_e$ plays a key role in understanding the optical and magnetic behavior of the system.

X-Ray and neutron diffraction are the usual techniques for the determination of internuclear distances in crystals. Nevertheless, these methods are not adequate for those cases in which M is a substitutional impurity in the crystal lattice. The extended X-ray-absorption fine-structure (EXAFS) technique can be used for the determination of the distance between the impurity and its nearest neighbors with great accuracy, although it needs relatively high impurity concentrations (of the order of 1%) (*1*). More recently, Moreno *et al.* have found that the equilibrium M–X distances can be

0022-4597/87 $3.00

obtained with great accuracy from the superhyperfine structure of the magnetic resonance spectra (*2–6*) or from the optical spectrum (*7*). Both methods seem to be useful for impurity concentrations as small as 1 ppm, and for concentrated materials as well.

From the theoretical side, a rather small number of nonempirical calculations of equilibrium metal–ligand distances in crystal lattices have been reported. We can mention the CNDO calculations of Clack and co-workers (*8*) on several MF_6^{n-} systems, whose results differ up to 20% from the experimental values; the more elaborated self-consistent-field molecular-orbital (SCF-MO) calculations of Pueyo and Richardson on K_2NaCrF_6 (*9*), Barandiarán and Pueyo on K_2NaCrF_6 and CrF_3 (*10*), and Miyoshi and Kashiwagi on $KCoF_3$, Cs_2CoF_6, and K_3CoF_6 (*11*), with theory–experiment agreements of about 1 to 6%. Also we can mention the multiple scattering $X\alpha$ (MS–$X\alpha$) calculations of Chermette and Pedrini (*12*) on $CuCl_6^{5-}$.

In spite of the good results in Refs. (*9*) and (*10*), we have recently reported (*13*) (henceforth referred to as I) the noticeable dependence of the cluster nuclear potential with the type of core–valence partition used. In I we presented calculations for the octahedral CrF_6^{4-} ion showing that (a) such dependence is a consequence of insufficient core–valence orthogonality in these frozen-core calculations and (b) the use of adequate core-projection operators in the frozen-core Hamiltonian enforces this orthogonality and gives rise to a near-partition-independent prediction of the equilibrium geometry.

In this work we extend the calculations to the CrF_6^{n-} (n = 2, 3, and 5) systems in an attempt to determine whether Richardson's methodology with core projection is able to give systematic predictions of the equilibrium properties of the 3*d* metal fluorides. We have analyzed the effects of the core projectors and the type and size of the core–valence partition in the curvature of the ground state nuclear potential. The effects in the cluster wavefunction have also been investigated.

All the calculations reported here are of the cluster-*in-vacuo* type. We do not include cluster-in-the-lattice calculations (*10*) because we want to show the accuracy of the cluster-*in-vacuo* description within a family of clusters. We have compared our results with more than 70 observed geometries. This calculation reveals that, in the worst cases, the cluster-*in-vacuo* values of R_e differ from the observed values by 0.1–0.2 Å. The totally symmetric cluster vibration $\bar{\nu}(a_{1g})$'s deviate, at most, by 100–150 cm^{-1}. Moreover, it appears that these deviations tend to coincide with the shifts expected from the cluster-lattice contribution (*10*). Therefore, the calculations reported in this work suggest that Richardson's methodology with core projection supplies cluster-*in-vacuo* descriptions useful in the study of families of compounds. On the other hand, rather elaborate cluster-in-the-lattice analyses might give a very accurate description of a particular system of interest. In our opinion, the two descriptions have then their own field of application. In the next section we give a short review of the method followed in the projected calculations. The study of the a_{1g} nuclear potentials of the fundamental states of the above-mentioned systems with and without core projection is presented in Section III. In the last section we present the comparison of the calculated equilibrium geometries with (some of) the available experimental data on chromium ions in fluoride lattices.

II. Richardson's Model with Core Projection

From paper I, we briefly recall that core-

projection operators try to enforce orthogonality among core and valence orbitals belonging to different centers. This constitutes a necessary condition for the electronic separation (*14, 15*).

The core-projection operators are defined in terms of symmetry-adapted orbitals (SAOs), $\chi(i\Gamma\gamma)$, as

$$\hat{\Omega}(\Gamma\gamma) = \sum_{i\epsilon\Gamma\gamma}^{\text{core}} B(i\Gamma)|\chi(i\Gamma\gamma)\rangle\langle\chi(i\Gamma\gamma)| \quad (1)$$

with

$$B(i\Gamma) = -x(i\Gamma)\varepsilon(i\Gamma) \quad (2)$$

where $\varepsilon(i\Gamma)$ are the energies of the corresponding core orbitals and $x(i\Gamma)$ the projection factors that, according to Höjer and Chung's theoretical analysis (*16*), should be taken as $x(i\Gamma) = 2$ (we will refer to other possible values in Sect. III). When the projection operator is incorporated in the unprojected effective one-electron Hamiltonian, H^{U}, one obtains the corresponding projected Hamiltonian, H^{P}.

As in paper I, we will use the quantity

$$E^{ortho}(R) = E^{\text{P}}(R) - E^{\text{U}}(R) \quad (3)$$

as a measure of the global effect of the core projection on the nuclear potential of an octahedral cluster. $E^{\text{P}}(R)$ and $E^{\text{U}}(R)$ are the total valence energy of the cluster in the projected and unprojected calculations, respectively. Furthermore, $E^{ortho}(R)$ can be divided into two contributions as follows:

(i) the expectation value of the core projector given by

$$E^{\Omega}(R) = \sum_{\Gamma}\sum_{i}\sum_{j\Gamma\gamma}^{\text{core}} n(i\Gamma\gamma)B(j\Gamma)|\langle\chi(j\Gamma\gamma)|\psi(i\Gamma\gamma)\rangle|^2 \quad (4)$$

where $n(i\Gamma\gamma)$ is the occupation number of $\psi(i\Gamma\gamma)$. This equation clearly shows that if the core–valence orthogonality is complete, $E^{\Omega}(R)$ vanishes.

(ii) the deformation energy, defined as

$$E^{\text{DEF}}(R) = E^{ortho}(R) - E^{\Omega}(R) \quad (5)$$

which measures the deformation, generated by the projection, of the valence electronic density.

In our calculations we have used the metallic bases of Richardson *et al.* (*17, 18*), except for the 4*s* AO that has been taken from Ref. (*9*). The fluoride basis has also been taken from Ref. (*9*). For consistency, the core projectors have been constructed with the same bases. The orbital energies of the metallic core AO's, needed in these calculations, have been taken from the atomic Hartree–Fock (HF) results of Watson (*19*), because Richardson's bases are simulations of Watson's. For the fluoride ion we have used the orbital energy of Clementi and Roetti (*20*).

We have considered in this work the three different core–valence partitions already defined in paper I: SPDD, SPDDSP, and DDSP. The prefixes U or P before the partition's name will refer to the unprojected or projected results, respectively.

III. Core Projection Results on Nuclear Potentials and Wavefunctions

We present now the calculations of the ground state nuclear potentials for the octahedral CrF_6^{n-} ($n = 2$, 3, and 5). Seven different Cr^{z+}–F^- distances have been used, the range depending on the charge of the chromium ion. In the case of Cr^+ we have used eight distances. These results can be compared with those for the $t_{2g}^3 e_g\text{-}^5E_g$ ground state of the CrF_6^{4-} ion studied in I.

Table I collects projected and unprojected results together with $E^{ortho}(R)$, $E^{\Omega}(R)$, and $E^{\text{DEF}}(R)$ for all cases. In order to facilitate the discussion, we depict in Fig. 1 $E^{\text{U}}(R)$ and $E^{\text{P}}(R)$ for the CrF_6^{n-} (n = 2–5) systems. To obtain the equilibrium

TABLE I

PROJECTED AND UNPROJECTED RESLTS FOR THE GROUND STATES OF THE CrF_6^{n-} (n = 2–5) IONS AT DIFFERENT Cr–F DISTANCES

			R (a.u.)						
			2.85	2.95	3.05	3.15	3.26	3.425	3.59
$(CrF_6)^{2-}$	SPDD	E^{U}	−0.65950	−0.82397	−0.91587	−0.95445	−0.95230	−0.89049	−0.78715
		E^{P}	−0.34168	−0.61337	−0.77522	−0.86001	−0.89104	−0.85821	−0.76996
		E^{ortho}	0.31782	0.21060	0.14065	0.09444	0.06126	0.03228	0.01719
		E^{Ω}	0.31441	0.20856	0.13939	0.09370	0.06084	0.03210	0.01710
		E^{DEF}	0.00341	0.00204	0.00126	0.00074	0.00042	0.00018	0.00009
	SPDDSP	E^{U}	−2.13290	−2.10171	−2.04719	−1.97551	−1.88267	−1.72648	−1.56074
		E^{P}	−1.37684	−1.49017	−1.54751	−1.56296	−1.54440	−1.46999	−1.36256
		E^{ortho}	0.75606	0.61154	0.49968	0.41255	0.33827	0.25649	0.19818
		E^{Ω}	0.56472	0.45367	0.37043	0.30764	0.25549	0.19929	0.15929
		E^{DEF}	0.19134	0.15787	0.12925	0.10491	0.08278	0.05720	0.03889
	DDSP	E^{U}	−3.68339	−3.23692	−2.87774	−2.58267	−2.31251	−1.98238	−1.71321
		E^{P}	−0.65997	−0.91744	−1.10403	−1.22920	−1.30767	−1.33616	−1.29142
		E^{ortho}	3.02342	2.31948	1.77371	1.35347	1.00484	0.64622	0.42179
		E^{Ω}	2.65744	2.09729	1.63898	1.26997	0.95233	0.61486	0.39949
		E^{DEF}	0.36598	0.22219	0.13473	0.08350	0.05251	0.03136	0.02230
			R (a.u.)						
			3.05	3.15	3.26	3.425	3.59	3.99	4.39
$(CrF_6)^{3-}$	SPDD	E^{U}	−0.41130	−0.50737	−0.56354	−0.57983	−0.54330	−0.35227	−0.12293
		E^{P}	−0.28624	−0.41051	−0.50005	−0.54576	−0.52482	−0.34791	−0.12185
		E^{ortho}	0.14306	0.09686	0.06349	0.03407	0.01848	0.00436	0.00108
		E^{Ω}	0.14071	0.09540	0.06265	0.03369	0.01831	0.00432	0.00104
		E^{DEF}	0.00235	0.00146	0.00084	0.00038	0.00017	0.00004	0.00004
	SPDDSP	E^{U}	−1.51907	−1.50092	−1.46325	−1.38217	−1.28192	−1.00238	−0.71126
		E^{P}	−1.02180	−1.09410	−1.13342	−1.13645	−1.09514	−0.90197	−0.65717
		E^{ortho}	0.48727	0.40682	0.32983	0.24572	0.18678	0.10041	0.05409
		E^{Ω}	0.36778	0.30357	0.25000	0.19215	0.15126	0.08789	0.04998
		E^{DEF}	0.11949	0.10325	0.07983	0.05357	0.03552	0.01252	0.00411
	DDSP	E^{U}	−2.36106	−2.11957	−1.90358	−1.64570	−1.43892	−1.04470	−0.71941
		E^{P}	−0.59268	−0.76984	−0.90222	−1.00426	−1.02335	−0.88711	−0.65172
		E^{ortho}	1.76838	1.34973	1.00136	0.64324	0.41557	0.15759	0.06769
		E^{Ω}	1.63402	1.26712	0.95022	0.61201	0.39522	0.14811	0.06402
		E^{DEF}	0.13436	0.08261	0.05114	0.03123	0.02035	0.00948	0.00367

			R (a.u.)						
			3.26	3.425	3.59	3.772	3.99	4.19	4.39
$(CrF_6)^{4-}$	SPDD	E^U	−0.57937	−0.68548	−0.73519	−0.74766	−0.72689	−0.68809	−0.63896
		E^P	−0.46452	−0.62105	−0.69847	−0.72764	−0.71710	−0.68297	−0.63628
		E^{ortho}	0.11485	0.06443	0.03672	0.02002	0.00979	0.00512	0.00268
		E^{Ω}	0.10983	0.06253	0.03599	0.01976	0.00972	0.00509	0.00267
		E^{DEF}	0.00502	0.00190	0.00073	0.00026	0.00007	0.00003	0.00001
	SPDDSP	E^U	−1.38682	−1.39874	−1.38581	−1.35071	−1.28891	−1.21961	−1.14247
		E^P	−1.03021	−1.14690	−1.20358	−1.22045	−1.20018	−1.15674	−1.09789
		E^{ortho}	0.35661	0.25184	0.18223	0.13026	0.08873	0.06287	0.04458
		E^{Ω}	0.27852	0.20242	0.15096	0.11147	0.07862	0.05723	0.04148
		E^{DEF}	0.07809	0.04942	0.03127	0.01879	0.01011	0.00564	0.00310
	DDSP	E^U	−1.84949	−1.67430	−1.54727	−1.43711	−1.32565	−1.23210	−1.14166
		E^P	−0.80255	−1.01248	−1.12636	−1.17790	−1.17657	−1.13968	−1.08285
		E^{ortho}	1.04694	0.66182	0.42091	0.25921	0.14908	0.09242	0.05881
		E^{Ω}	0.99308	0.63367	0.40306	0.24716	0.14154	0.08774	0.05606
		E^{DEF}	0.05386	0.02815	0.01785	0.01205	0.00754	0.00468	0.00275

			R (a.u.)							
			3.26	3.425	3.59	3.99	4.19	4.39	4.59	4.99
$(CrF_6)^{5-}$	SPDD	E^U	−1.15765	−1.33504	−1.46117	−1.63390	−1.67831	−1.70632	−1.72262	−1.73184
		E^P	−0.86526	−1.15803	−1.35222	−1.59884	−1.65819	−1.69475	−1.71602	−1.72968
		E^{ortho}	0.29239	0.17701	0.10895	0.03506	0.02012	0.01157	0.00660	0.00216
		E^{Ω}	0.26337	0.16545	0.10429	0.03451	0.01992	0.01148	0.00660	0.00216
		E^{DEF}	0.02902	0.01156	0.00469	0.00055	0.00020	0.00009	0.00000	0.00000
	SPDDSP	E^U	−1.85485	−1.94691	−2.01534	−2.10141	−2.11360	−2.11136	−2.09785	−2.04660
		E^P	−1.36031	−1.61392	−1.78673	−2.00430	−2.04932	−2.06871	−2.06959	−2.03441
		E^{ortho}	0.49454	0.33299	0.22861	0.09711	0.06428	0.04265	0.02826	0.01219
		E^{Ω}	0.40409	0.28164	0.19875	0.08873	0.05984	0.04032	0.02705	0.01189
		E^{DEF}	0.09045	0.05135	0.02986	0.00838	0.00444	0.00233	0.00121	0.00030
	DDSP	E^U	−2.32726	−2.22315	−2.17157	−2.12542	−2.11175	−2.09538	−2.07417	−2.01658
		E^P	−1.11118	−1.46096	−1.69236	−1.96452	−2.01624	−2.03770	−2.03883	−2.00292
		E^{ortho}	1.21608	0.76219	0.47921	0.16090	0.09551	0.05768	0.03534	0.01366
		E^{Ω}	1.13855	0.72737	0.46052	0.15464	0.09186	0.05561	0.03422	0.01337
		E^{DEF}	0.07753	0.03482	0.01869	0.00626	0.00365	0.00207	0.00112	0.00029

Note. All numbers are in a.u. E^P and E^U are valence energies +225 a.u. for CrF_6^{2-} and CrF_6^{3-}, +224 for CrF_6^{4-}, and +222 a.u. for CrF_6^{5-}. Core energies of the 3*s* and 3*p* AO's have been added up to the valence energy in the DDSP results to make the comparison with other partitions easier.

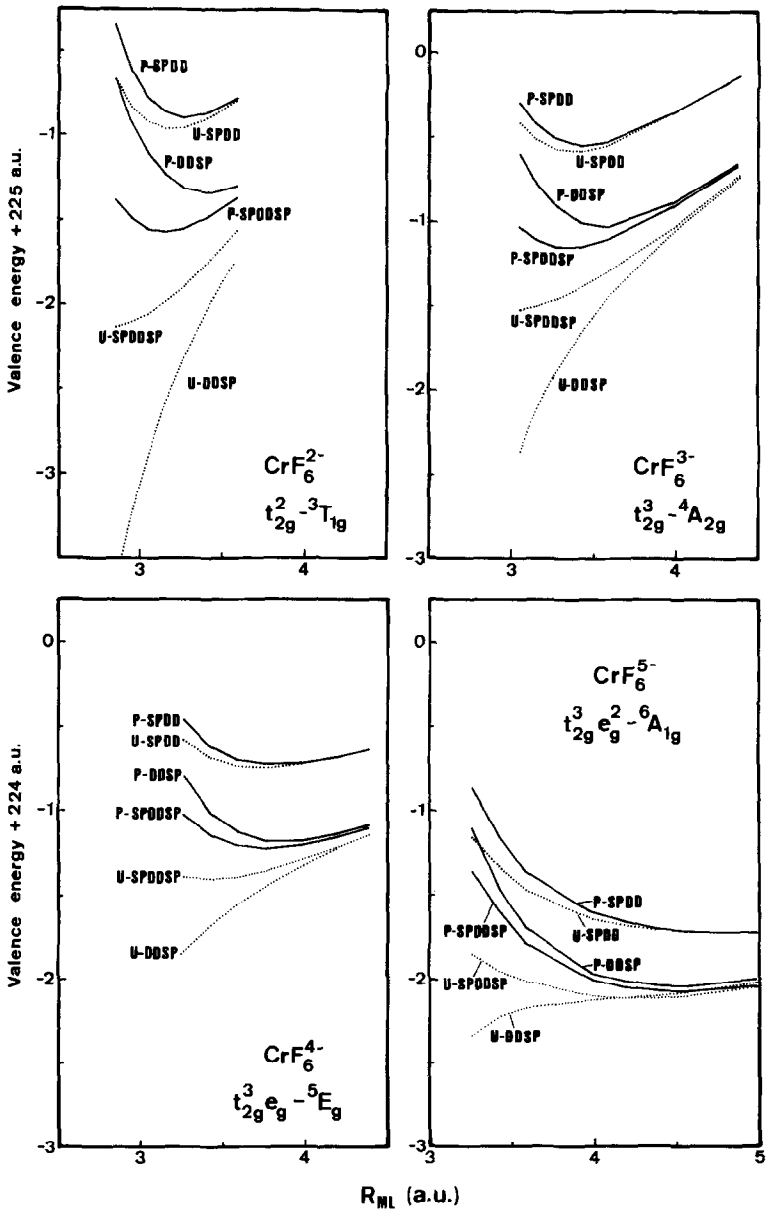

FIG. 1. Projected and unprojected ground state nuclear potentials for the CrF_6^{n-} (n = 2–5) ions.

properties, we write the SCF valence energy in the form,

$$E(R) = E(\infty) + V_{\text{ion}}(R) + E_{\text{nc}}(R) \quad (6)$$

where $E(\infty)$ is the energy of the infinitely separated ions ($Cr^{z+} + 6F^-$), $V_{\text{ion}}(R)$ the intracluster interaction in the point charge approximation: $V_{\text{ion}}(R) = 6[\sqrt{2} + \frac{1}{4} - (6 - n)]/R$ for the MF_6^{n-} unit, and $E_{\text{nc}}(R)$ the nonelectrostatic energy. $E_{\text{nc}}(R)$ can be accurately represented by the function,

$$E_{\text{nc}}(R) = AR^{-m} + BR^{-1}e^{-nR}. \quad (7)$$

Using $E(\infty)$, A, B, m, and n as fitting pa-

rameters we find the values of R_e and $\bar{\nu}(a_{1g})$ collected in Table II.

Unprojected Results

Let us comment briefly on the unprojected results, some of them previously reported by our group (*9, 21, 22*). As can be seen in Fig. 1, in all these clusters there are large differences among the nuclear potentials corresponding to the three core–valence partitions.

The U-SPDD partition predicts stable states in three cases, with equilibrium distances: $R_e(CrF_6^{2-})$ = 3.197 a.u., $R_e(CrF_6^{3-})$ = 3.381 a.u., and $R_e(CrF_6^{4-})$ = 3.748 a.u. In CrF_6^{5-} there are no signs of a stable ground state, at least in the range of distances explored here (up to 5 a.u.).

The U-SPDDSP partition produces a substantial decrease of the equilibrium distance (about 10–14%): $R_e(CrF_6^{2-})$ = 2.799 a.u., $R_e(CrF_6^{3-})$ = 3.005 a.u., $R_e(CrF_6^{4-})$ = 3.413 a.u., and $R_e(CrF_6^{5-})$ = 4.253 a.u. As we discuss below, this big reduction of R_e in passing from U-SPDD to U-SPDDSP calculations is due mainly to the lack of orthogonality between the 4*s* and 4*p* metallic AO's and the $1s_F$ core AO's of the fluorides.

The U-DDSP results are even more striking: the SCF nuclear potentials become attractive down to the lowest distance explored. We will see below that this behavior is a consequence of the lack of orthogonality between the $3s_M$ and $3p_M$ core AO's and the $2s_F$ and $2p_F$ valence AO's.

Projected Results

We will now comment on the results of the projected calculations. As a general result, we note first that the core projection increases the energy of the system, i.e., $E^{ortho}(R)$ is always positive. This can be seen in Table I. Since this increase in energy is bigger at smaller metal–ligand distances, the core projection increases the value of R_e. The curvature of the nuclear potential in the equilibrium region also increases, giving rise to larger values of $\bar{\nu}(a_{1g})$, as can be seen in Table II. Another general result is that the main contribution

TABLE II

EQUILIBRIUM DISTANCES R_e (Å), AND a_{1g} VIBRATION FREQUENCIES, $\bar{\nu}(cm^{-1})$, OF THE CrF_6^{n-} (n = 2–5) IONS (NUMBERS IN PARENTHESES ARE EXTRAPOLATIONS)

Cluster	Ground state	Core–valence partition	R_e (Å)		$\bar{\nu}(cm^{-1})$	
			U-	P-	U-	P-
CrF_6^{2-}	t_{2g}^2–$^3T_{1g}$	SPDD	1.692	1.733	878	878
		SPDDSP	(1.481)	1.664	(910)	851
		DDSP	—	1.798	—	832
CrF_6^{3-}	t_{2g}^3–$^4A_{2g}$	SPDD	1.789	1.823	711	711
		SPDDSP	(1.590)	1.773	(717)	678
		DDSP	—	1.883	—	703
CrF_6^{4-}	$t_{2g}^3e_g$–^5E_g	SPDD	1.983	2.020	455	463
		SPDDSP	1.806	1.992	461	475
		DDSP	—	2.047	—	516
CrF_6^{5-}	$t_{2g}^3e_g^2$–$^6A_{1g}$	SPDD	—	—	—	—
		SPDDSP	2.251	2.375	280	292
		DDSP	—	2.375	—	304

to $E^{ortho}(R)$ comes from the expectation value of the projector $E^{\Omega}(R)$, whereas $E^{DEF}(R)$ contributes from 1 to about 25%, depending on the distance and partition used. This fact suggests that neither the MO's nor the properties that depend on the shape of the valence MO's are much affected by the projection. We discuss this effect below. Let us see first the results of the projection on the nuclear potentials.

In the SPDD partition, E^{ortho} is quite small, much smaller than in the other partitions, so that the U- and P-SPDD nuclear potentials are very similar in the equilibrium region. The differences $\Delta R = R_e$(P-SPDD) $- R_e$(U-SPDD) are: 0.077 (CrF_6^{2-}), 0.064 (CrF_6^{3-}), and 0.070 a.u. (CrF_6^{4-}). As in the U-SPDD calculations, the P-SPDD nuclear potential of CrF_6^{5-} is continuously repulsive in the range of distances studied (3.26–4.99 a.u.). E^{ortho} and $E^{\Omega}(R)$ steeply decrease as R increases, following R^{-11} or R^{-13} laws for these clusters. $E^{DEF}(R)$ represents 2% or less of the total $E^{ortho}(R)$ value, and decreases quickly with increasing distance (as R^{-15}–R^{-20}). This energy is practically negligible in the equilibrium region.

The projection effects are much more important in the SPDDSP partition. E^{ortho}(P-SPDDSP) is much larger than E^{ortho}(P-SPDD) at all distances, and the same happens with $E^{\Omega}(R)$ and $E^{DEF}(R)$. The U- and P-SPDDSP nuclear potentials are very different in the equilibrium region. So, ΔR = 0.35 (CrF_6^{2-}), 0.35 (CrF_6^{3-}), 0.352 (CrF_6^{4-}), and 0.24 a.u. (CrF_6^{5-}). $E^{ortho}(R)$ decreases as an inverse power of the metal–ligand distance, with larger exponent for larger central ion charge: $R^{-5.8}$ (CrF_6^{2-}), $R^{-6.0}$ (CrF_6^{3-}), $R^{-6.9}$ (CrF_6^{4-}), and $R^{-8.6}$ (CrF_6^{5-}). $E^{\Omega}(R)$ is the biggest contribution to $E^{ortho}(R)$. It decreases with R in a slower way than $E^{ortho}(R)$: $R^{-5.5}$ (CrF_6^{2-}), $R^{-5.4}$ (CrF_6^{3-}), $R^{-6.3}$ (CrF_6^{4-}), and $R^{-8.2}$ (CrF_6^{5-}). $E^{DEF}(R)$ is smaller but it can be up to 25% of $E^{ortho}(R)$ at small distances. Thus, the projector effect over the valence MO's can be relatively important in this partition. On the other hand, $E^{DEF}(R)$ decreases quickly with increasing distance: $R^{-6.9}$ (CrF_6^{2-}), $R^{-9.3}$ (CrF_6^{3-}), $R^{-10.8}$ (CrF_6^{4-}), and $R^{-13.1}$ (CrF_6^{5-}).

Finally, the results of the projection in the DDSP partition are dramatic. All the U-DDSP calculations predict nuclear potentials continuously attractive in the range of distances studied here, a result rather unsatisfactory. Core projection corrects this image and produces nuclear potentials comparable to those obtained with the other two partitions. As before, $E^{ortho}(R)$ deceases with increasing R: $R^{-8.6}$ (CrF_6^{2-}), $R^{-9.0}$ (CrF_6^{3-}), $R^{-9.7}$ (CrF_6^{4-}), and $R^{-10.5}$ (CrF_6^{5-}). The contribution of $E^{DEF}(R)$ to $E^{ortho}(R)$ goes from 2 to 12%, depending on the distance considered. We observe that E^{DEF}(SPDDSP) > E^{DEF}(DDSP) at the calculated equilibrium distances, but this relation can be reversed at much smaller distances, as a consequence of the different slope of the $E^{DEF}(R)$ function in both partitions. So, although the projection effects on the nuclear potentials are much bigger in the DDSP than in the SPDDSP case (E^{ortho}(SPDDSP) < E^{ortho}(DDSP) for all distances considered here), the effects on the shape of the valence MO's in the equilibrium regions are bigger in the SPDDSP partition. The latter result may be a consequence of the larger flexibility of the SPDDSP bases.

It is interesting to note that the P-SPDD and P-SPDDSP nuclear potentials are practically parallel (see Fig. 1). The P-SPDDSP potentials always lie below the P-SPDD ones, as they correspond to a larger and variationally more efficient basis. The P-DDSP potential, however, differs noticeably from the other two. In CrF_6^{5-} we have a somewhat different picture: the P-DDSP potential is practically parallel to the P-SPDDSP in the equilibrium region.

Analysis of the Projection Effect

As commented above, the small values of

$E^{DEF}(R)$ indicate small effects of the core projection on the valence charge distributions of these clusters. This interesting result could be related to the fact that the basis used in the calculations is composed of valence AO's which are orthogonal to core AO's of the same center. In fact, the valence AO's have the characteristic radial and angular nodes of the atom and, consequently, the MO's obtained as linear combinations of them can have all the nodes that the all electron MO's would have.

In order to illustrate this argument we have depicted in Fig. 2a, as an example, the valence MO's of the a_{1g} block obtained in the U-SPDDSP calculation of CrF_6^{4-} at R = 3.26 a.u. It can be seen that the $4a_{1g}(\sim 3s_M)$, $5a_{1g}(\sim 2s_L)$, and $6a_{1g}(\sim 2p_{\sigma L})$ MO's have the characteristic nodal regions that would enforce, in the all-electron case, orthogonality to the core $1s_M(\sim 1a_{1g})$, $2s_M(\sim 2a_{1g})$, and $1s_L(\sim 3a_{1g})$ AO's. Inclusion of the core projection does not make big changes, as Fig. 2b illustrates. There is only a slight decrease in the charge density of the $6a_{1g}$ at the nucleus and inner region of the F^- ion, compensated by a slight increase in the near outer region. Similar results are obtained for the other blocks, partitions, and distances.

It is important to remark that despite the adequate nodal structure of the valence MO's, core–valence orthogonality is not completely reached. This lack of orthogonality remains after projection due to insufficient flexibility of the basis set. It should affect the energy calculation, since the usual equation $E_{val} = \langle \Phi_{val}(1 \ldots Nv) | \hat{H}_{val} | \Phi_{val}(1 \ldots Nv) \rangle$, where $\Phi_{val}(1 \ldots Nv)$ is the valence multielectronic wavefunction, is incorrect if core–valence orthogonality fails (*14, 15, 23*). The inclusion of $E^{\Omega}(R)$ in the valence energy works as an approximate correction to this residual nonorthogonality (*24*).

As a final remark, we would like to comment on the best values of the projection constant $x(i\Gamma)$ in Eq. (2). Our recent studies on the projection effects in frozen-core atomic calculations (*24*) suggest the convenience of a softer projection [$x(i\Gamma) \sim 1$] when the valence basis does not have enough flexibility in the regions of high core electronic density. This prevents excessive outward shifts of the valence orbitals affected by projection. The use of soft core projection has also been invoked by other authors (see for instance (*25–27*) to improve the agreement between molecular calculations with model potential or effective core potentials and the corresponding all-electron calculations. In these cases, however, the problems were attributed to the difficulty of reproducing core–valence exchange interactions. In the molecular calculations reported here, these problems should be negligible, given the small effect of the projector on the valence MO's shape. Nevertheless, in order to study the significance of the $x(i\Gamma)$'s, we have carried out calculations using reduced projection constants. Figure 3 depicts the nuclear potentials obtained in the CrF_6^{4-} case. The projection constants used are indicated in parentheses as $(x_1 \ldots x_n, y_2 \ldots y_n, z_1)$, where x_i, y_i stand for the metallic is_M and ip_M AO's, respectively, and z_1 for the ligand $1s_L$ AO.

As can be seen in Fig. 3, reduction of $x(1s_M)$, $x(2s_M)$, and $x(2p_M)$ from 2 to 1 does not significantly change the nuclear potentials in any partition. On the contrary, the value of $x(1s_F)$ tuns out to be of great importance in the SPDDSP and the DDSP partitions. This can be seen in Figs. 3b and c, where one can classify the nuclear potentials in families depending on the value of $x(1s_F)$. Such a result can be explained as a consequence of the large overlap between the $1s_F$ AO and the $3d$, $4s$, and $4p$ metallic AO's (see Fig. 4). In the DDSP partition, the projection of the $3s$ and $3p$ AO's is even more important. Again, this is a consequence of the size of their

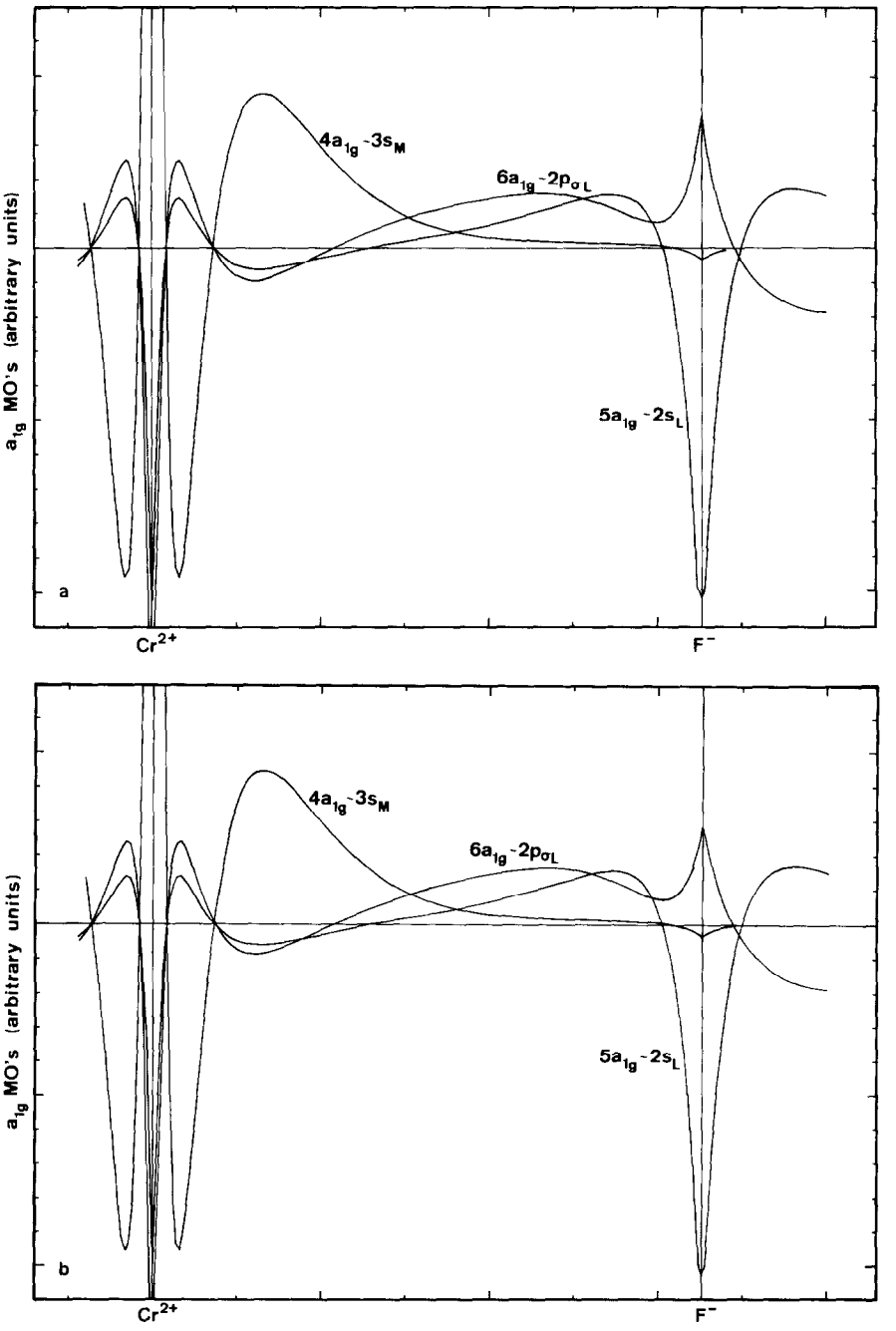

FIG. 2. a_{1g} MO's from (a) U-SPDDSP and (b) P-SPDDSP solutions of the $t_{2g}^3 e_g$-^5E_g ground state of the CrF_6^{4-} ion at R = 3.26 a.u.

overlap with the fluoride $2s_F$ and $2p_F$ AO's (Fig. 4).

In conclusion we can say that the values assigned to the projection constants depend largely on the overlap between the corresponding core function and the valence

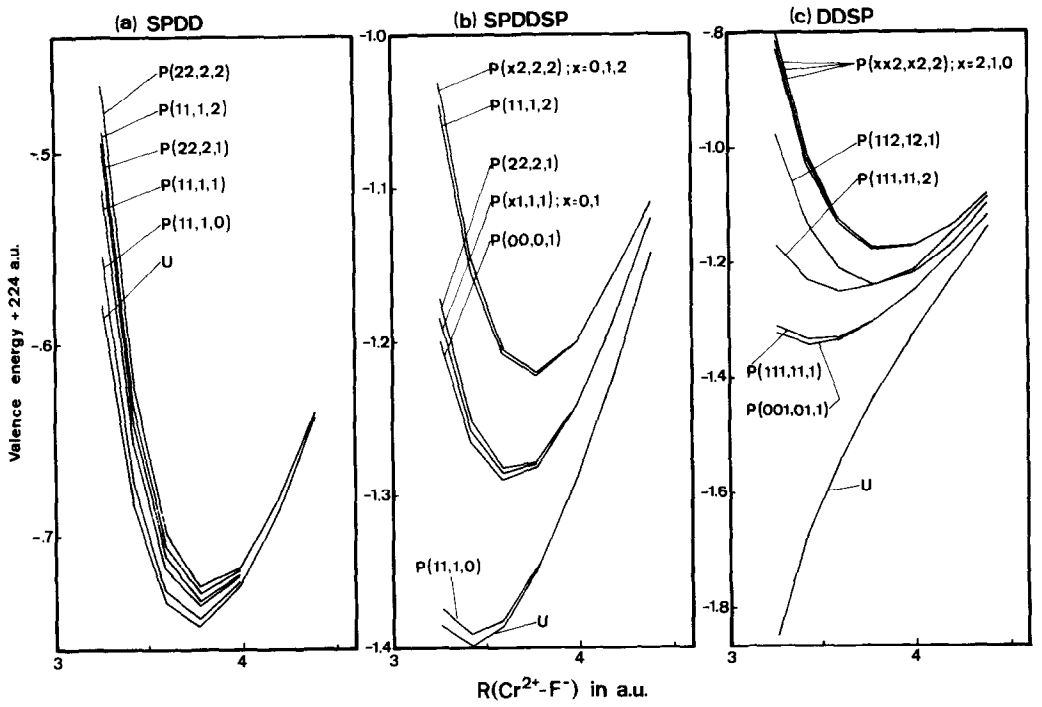

FIG. 3. Nuclear potentials of the ground state of the CrF_6^{4-} ion obtained with different projection constants $x(i\Gamma)$. DDSP results include the contribution of the 3*s* and 3*p* core AO's.

shell. When this overlap is small, any value from 1 to 2 seems to work adequately. In cases of larger overlap the softer projection should be avoided in order to obtain good consistency among nuclear potentials of different partitions.

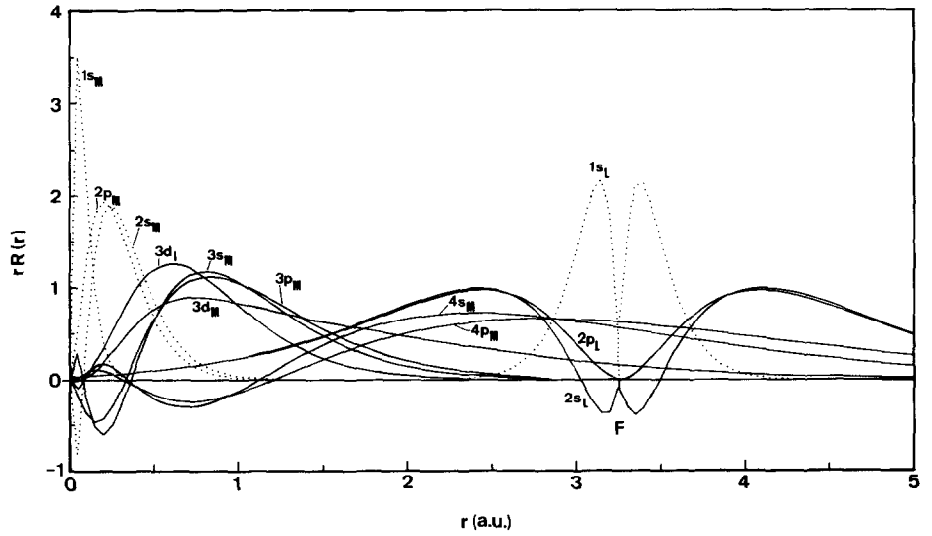

FIG. 4. Radial parts of metallic and fluoride AO's at $R = 3.26$ a.u. Dotted lines have been used for core AO's, solid lines for valence AO's.

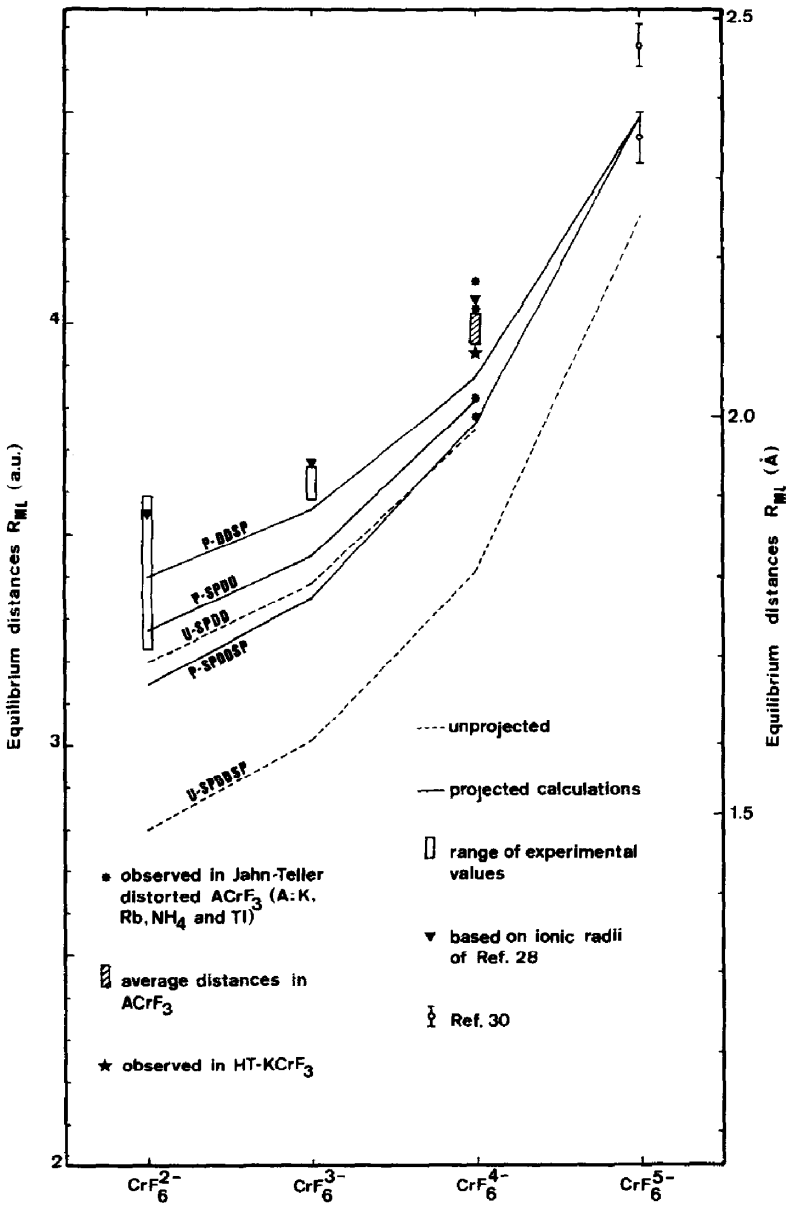

FIG. 5. Equilibrium distances of the CrF_6^{n-} (n = 2–5) systems.

IV. Equilibrium Properties: Comparison between In-Vacuo Calculations and Experimental Values

In this section we compare our calculated equilibrium distances with those observed in several ionic crystals.

As mentioned in the previous section, equilibrium distances and $\bar{\nu}(a_{1g})$ frequencies, collected in Table II, have been deduced from the optimized function given by Eq. (6). In Fig. 5 we show the theoretical and experimental equilibrium distances, and in Fig. 6 the calculated frequencies.

In Fig. 5 we can observe the great regularity of the calculated R_e's as functions of

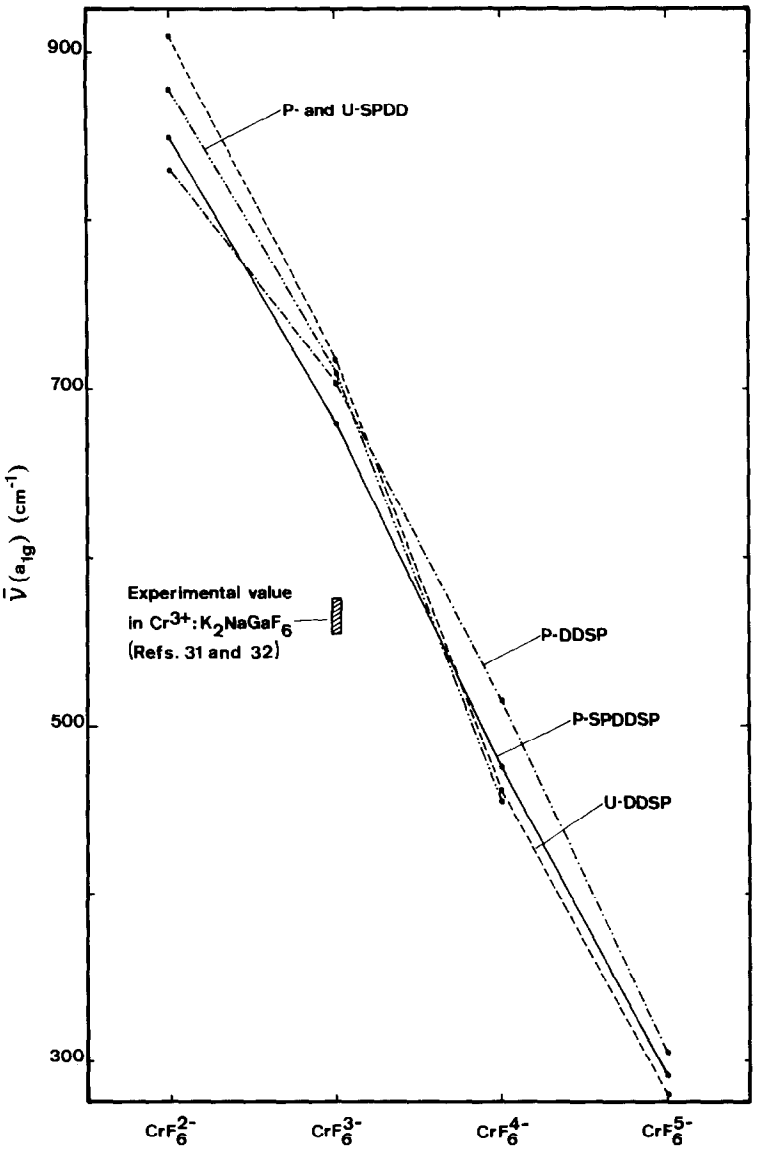

FIG. 6. Calculated $\bar{\nu}(a_{1g})$'s for the CrF_6^{n-} (n = 2–5) systems.

the cluster's charge. R_e increases with n, in agreement with the trend shown by the ionic radii of the metal (*28*).

Equilibrium distances obtained with the three core–valence partitions are in good agreement. Inclusion of the 4*s* and 4*p* virtual valence AO's of the metal decreases R_e, probably because these AO's increase the electronic delocalization and the metal–fluoride interaction. On the contrary, R_e appreciably increases when the 3*s* and 3*p* AO's are included in the core, indicating the contribution of these AO's to the metal–fluoride bond. In $(CrF_6^{3-}$, for instance, R_e(P-DDSP) − R_e(SPDDSP) = 0.11 Å, a change comparable to the crystal lattice effects described in K_2NaCrF_6 (*10*). On the other hand, the dispersion among equilibrium distances calculated in different partitions increases with the central ion's

charge, revealing that the contribution of the $3s$, $3p$, $4s$, and $4p$ AO's to the metal–fluoride bonding in these clusters increases with the metal ionization.

The equilibrium $R_e(Cr^{n+}-F^-)$ distances have been determined by diffraction methods in numerous crystals. In Tables III to V we have collected a significant part of the available experimental information that will be used to examine our theoretical results.

As can be see in Table III, the CrF_6^{2-} system appears as a slightly distorted octahedron in $M^{2+}CrF_6$- and $M_2^+CF_6$-type compounds, where the equilibrium $Cr^{4+}-F^-$ distance varies from 1.71 to 1.86 Å. Our theoretical values, corresponding to the P-SPDD (~1.73 Å) and P-DDSP (~1.80 Å) calculations, are within the experimental range, the P-SPDDSP values being smaller (~1.66 Å).

Table IV presents a great variety of reliable experimental data on the $Cr^{3+}-F^-$ distance. It can be seen that the CrF_6^{3-} unit shows a great preference for the regular octahedral structure and that the $Cr^{3+}-F^-$ distance varies from 1.89 to 1.94 Å. Our theoretical P-SPDD (1.823 Å) and P-SPDDSP (1.773 Å) results are 0.1–0.2 Å smaller than the observed ones. The P-DDSP value, R_e = 1.883 Å, practically coincides with the lower limit of the experimental range.

The ^5E_g octahedral ground state of the CrF_6^{4-} ion is expected to undergo a strong Jahn–Teller splitting. It is observed so in $KCrF_3$, where the CrF_6^{4-} cluster takes the shape of an enlarged octahedron with two equatorial fluorides at 1.946 Å, two at 2.002 Å, and two axial fluorides at 2.332 Å. That means an average $Cr^{2+}-F^-$ distance of 2.09 Å. We want to emphasize that Cousseins and De Kozak (*29*) reported a phase transition on $KCrF_3$, produced by a lengthy heating at 500°C, to a perovskite-type cubic lattice in which the Cr^{2+} ion is surrounded by a regular octahedron of fluorides at 2.08 Å. The fact that the observed distance for this octahedral CrF_6^{4-} coincides with the average value quoted above makes plausible the use of these averages in distorted clusters. From Table V we can estimate a range of 2.08–2.13 Å for the $Cr^{2+}-F^-$ distance in octahedral compounds of Cr^{2+}. The theoretical distances computed in this work are slightly smaller than the observed average values, as can be seen in Fig. 5. The fact that R_e(P-SPDD) = 2.020 Å, R_e(P-SPDDSP) = 1.992 Å, and R_e(P-DDSP) = 2.047 Å do compare well with the smaller distances in JT-distorted octahedra (ranging from 1.95 to 2.02 Å) is probably fortuitous. However it is satisfactory to see that the differences between our *in-vacuo* values and the observed average distances are only 0.05–0.14 Å.

Finally, there are not, to our knowledge, stable compounds of Cr^+ in fluoride lattices. Nevertheless, the equilibrium distance of the CrF_6^{5-} cluster has been estimated from the observed isotropic superhyperfine constant, A_s, in $Cr^+:KMgF_3$ (R_e = 2.35 ± 0.02 Å), and in $Cr^+:NaF$ (R_e = 2.47 ± 0.02 Å) (*30*). Our calculations predict an equilibrium distance of 2.38 Å in both P-SPDDSP and P-DDSP partitions.

Let us now comment on our results on vibrational frequencies. We show them in Fig. 6. It can be observed that $\bar{\nu}(a_{1g})$ increases when the charge of the central metal increases, as could be expected. The calculated $\bar{\nu}(a_{1g})$ strongly depends on the type of nuclear potential function used for representing the SCF results, as well as on the quality of the fitting. However, we notice that the values obtained with different core–valence partitions are very similar. To our knowledge, the only experimental data available for these systems refer to the CrF_6^{3-} cluster. Ferguson *et al.* (*31*) have determined $\bar{\nu}(a_{1g})$ = 568 ± 4 cm^{-1} from the fluorescence spectra of $Cr^{3+}:K_2NaGaF_6$. Dubicki *et al.* (*32*) obtained $\bar{\nu}(a_{1g})$ = 575 cm^{-1} from the analysis of the vibrational structure of the $^4A_{2g} \leftarrow {}^2E_g$ emission and 564 cm^{-1} from the Raman spectrum of this sys-

TABLE III

OBSERVED GEOMETRIES OF CrF_6^{2-}-CONTAINING SYSTEMS

Compound	Method	Symmetry	Space group	Z	Lattice constant	M–F distance (Å)	M–F average distance	Reference
$KCrF_5$	P	Hexag		3	$a = 8.739$, $c = 5.226$			33, 34
$RbCrF_5$	P	Hexag		3	$a = 6.985$, $c = 12.12$			33, 34
$CsCrF_5$	P	Cubic		4	$a = 8.107$			33, 34
Li_2CrF_6	P	Monoc	$P2_1/c$	2	$a = 4.587$, $c = 9.993$, $\beta = 117.27°$	2 × (1.662, 1.711, 1.748)	1.71	35
Na_2CrF_6	P	Trig	$P321$	3	$a = 9.14$, $c = 5.15$	6 × (1.722)	1.72	34
HT-K_2CrF_6	P	Cubic	$Fm3m$	4	$a = 8.105$	6 × (1.662)	1.66	33, 34
K_2CrF_6	P	Hexag	$P6_3mc$	2	$a = 5.70$, $c = 9.35$	3 × (1.749, 1.776)	1.76	36, 34
Rb_2CrF_6	P	Hexag	$P6_3mc$	2	$a = 5.95$, $c = 9.69$	3 × (1.82, 1.85)	1.84	36, 34
Cs_2CrF_6	P	Cubic	$Fm3m$	4	$a = 8.196$ or $a = 9.022$	6 × (1.828) or 6 × (1.850)	1.83–1.85	33, 36
$BaCrF_6$	P	Hexag			$a = 7.328$, $c = 7.137$	( )1.83, ( )1.84		37
$SrCrF_6$	P	Hexag			$a = 7.109$, $c = 6.863$	( )1.81, ( )1.79		37
$CaCrF_6$	P	Rhomb			$a = 5.336$, $c = 14.153$	( )1.90, ( )1.92		37
$MgCrF_6$	P	Rhomb			$a = 5.091$, $c = 13.143$	( )1.85, ( )1.87		37
$CdCrF_6$	P	Rhomb			$a = 5.140$, $c = 14.075$	( )1.85, ( )1.84		37
$HgCrF_6$	P	Rhomb			$a = 5.128$, $c = 14.265$	( )1.89, ( )1.87		37
$NiCrF_6$	P	Rhomb			$a = 4.975$, $c = 13.262$	( )1.90		37
$ZnCrF_6$	P	Rhomb			$a = 5.026$, $c = 13.337$	( )1.88		37

Note. HT = high temperature; P = powder diagram.

TABLE IV

OBSERVED GEOMETRIES OF CrF_6^{3-}-CONTAINING SYSTEMS

Compound	Method	Symmetry	Space group	Z	Lattice constant	M–F distance (Å)	M–F average distance	Reference
CrF_3	*	Rhomb	$R\bar{3}c$	2	$a = 5.264 \pm 0.001$, $\alpha = 56.609 \pm 0.006$	6 × (1.90)	1.90	38
$KCrF_4$	*	Orthor	$Pnma$	24	$a = 15.76$, $b = 7.43$, $c = 18.38$	2 × (1.860), 4 × (1.934)	1.91	39
$CsCrF_4$	*	Hexag	$P\bar{6}2m$	3	$a = 9.650$, $c = 3.857$	2 × (1.851, 1.929, 1.940)	1.91	40
Rb_2CrF_5	*	Orthor	$Pnma$	4	$a = 7.515$, $b = 5.724$, $c = 11.985$	2 × (1.990, 1.862), 1.903, 1.852	1.91	41
$CaCrF_5$	*	Monoc[a]	$C2/c$	4	$a = 9.005$, $b = 6.472$, $c = 7.533$, $\beta = 115.85°$	2 × (1.940, 1.918, 1.848)	1.90	42, 43
$SrCrF_5$	P	Orthor		4	$a = 9.700$, $b = 7.807$, $c = 7.087$			44
$CdCrF_5$	P	Orthor		16	$a = 20.30$, $b = 9.97$, $c = 7.47$			45
$MnCrF_5$	*	Monoc	$C2/c$	4	$a = 8.586$, $b = 6.291$, $c = 7.381$, $\beta = 115.46°$	2 × (1.913, 1.900, 1.870)	1.89	46
K_2NaCrF_6	*	Cubic	$Fm3m$	4	$a = 8.266$	6 × (1.933 ± 0.011)	1.93	47
Cs_2KCrF_6		Cubic	$Fm3m$	4	$a = 9.004$	6 × (1.936)	1.94	48
Rb_2KCrF_6		Cubic	$Fm3m$	4	$a = 8.817$	6 × (1.94)	1.94	48
Rb_2NaCrF_6		Cubic	$Fm3m$	4	$a = 8.418$	6 × (1.94)	1.94	48
Cs_2NaCrF_6	*	Rhomb	$R\bar{3}m$	6	$a = 6.243$, $c = 30.33$	6 × (1.906) and 6 × (1.913)	1.91	49, 50
HPT-Cs_2NaCrF_6		Cubic[b]	$Fm3m$	4	$a = 8.706$	6 × (1.95 ± 0.05)		51
HPT-Cs_2NaCrF_6		Hexag[c]			$a = 6.213$, $c = 15.11$			51
Na_3CrF_6	*	Monoc	$P2_1/c$	2	$a = 9.6618(9)$, $b = 5.7021(3)$, $c = 5.4913(3)$, $\beta = 125.021(5)°$	2 × (1.904, 1.907, 1.909)	1.907	52
K_3CrF_6	P	Cubic	$Fm3m$	4	$a = 8.54$	6 × (1.84) ?		53
$RbNiCrF_6$	*	Cubic	$Fd3m$	8	$a = 10.21$	6 × (1.91)	1.91	54
$KNiCrF_6$	P*	Cubic	$Fd3m$	8	$a = 10.24$	6 × (1.93)	1.93	54
$KNiCrF_6 \cdot H_2O$	P*	Cubic	$Fd3m$	8	$a = 10.45$	6 × (1.94)	1.94	54
$LiCaCrF_6$	P	Trig	$P\bar{3}1c$	2	$a = 5.095$, $c = 9.720$			55
$LiSrCrF_6$	P	Trig	$P\bar{3}1c$	2	$a = 5.170$, $c = 10.34$			55
$LiCdCrF_6$	P	Trig	$P\bar{3}1c$	2	$a = 5.086$, $c = 9.495$			55
$LiBaCrF_6$	*	Monoc	$P2_1/c$	4	$a = 5.397(3)$, $b = 10.355(5)$, $c = 8.638(5)$, $\beta = 90.72(5)°$	1.917, 1.933, 1.904, 1.876, 1.910, 1.878	1.903	56
$NaMnCrF_6$	*	Trig	$P321$	3	$a = 8.993(1)$, $c = 5.003(1)$	6 × (1.909) 3 × (1.905, 1.912)	1.909 1.909	57
Na_2MgCrF_7	*	Orthor	$Imm2$	4	$a = 7.39$, $b = 7.15$, $c = 10.20$			58
$KPbCr_2F_9$	*	Orthor	$Pnma$	4	$a = 9.812$, $b = 5.412$, $c = 13.93$	2 × (1.872, 1.917), 1.887, 1.927 2 × (1.912, 1.890), 1.862, 1.922	1.90 1.90	59

Note. HPT = high temperature and pressure; * = singe crystal; P = powder diagram; P* = powder diagram plus refinements.

[a] Assignment of Ref. (*43*).

[b] Observed at 30 kbar and 600°C.

[c] Observed at 25 kbar and 800°C.

TABLE V

OBSERVED GEOMETRIES OF CrF_6^{4-}-CONTAINING SYSTEMS

Compound	Method	Symmetry	Space group	Z	Lattice constant	M–F distance (Å)	M–F average distance	Reference
CrF_2		Monoc	$P2_1/n$	2	a = 4.732, b = 4.718, c = 3.505, β = 96.5°	2 × (1.98, 2.01, 2.43)	2.14	60, 61
$KCrF_3$[a]	P	Tetrag	*I4/mcm*	4	a = 6.036, c = 8.010	2 × (1.946, 2.002, 2.322)	2.09	29, 34, 62
HT-$KCrF_3$[b]	P	Cubic	*Pm3m*	1	a = 4.158(4)	6 × (2.079 ± 0.002)	2.08	29, 63
$RbCrF_3$[c]	P	Tetrag	*I4/mcm*	4	a = 6.149, c = 8.088	2 × (1.983, 2.22, 2.365)	2.12	29, 34
NH_4CrF_3	P	Tetrag	*I4/mcm*	4	a = 6.232, c = 7.954	2 × (1.988, 2.010, 2.397)	2.13	34
$TlCrF_3$	P	Tetrag	*I4/mcm*	4	a = 6.194, c = 8.064	2 × (1.997, 2.016, 2.383)	2.13	34
Na_2CrF_4		Monoc	$P2_1/c$	2	a = 3.344, b = 9.533, c = 5.657, β = 87.2°	2 × (1.933, 1.947, 2.424)	2.10	34, 64
$SrCrF_4$[d]	*	Tetrag	*I4/mcm*	4	a = 5.673(3), c = 10.920(6)	4 × (1.981) square planar		65, 66
$CaCrF_4$[e]	*	Tetrag	*I4/mcm*	4	a = 5.45(2), c = 10.62(2)	4 × (1.914)		44
$BaCrF_4$		Tetrag	?	18	a = 15.59(1), c = 7.66(1)			44
Ba_2CrF_6		Monoc	*I2/m*	2	a = 4.245(5), b = 16.20(1), c = 4.245(5), β = 92.20(5)°			44

Note. HT = high temperature; * = single crystal; P = powder diagram.

[a] Assignment of Ref. (*34*).

[b] Observed after heating at 500°C.

[c] Assignment of Ref. (*34*) with data from Ref. (*29*) by analogy with $KCrF_3$.

[d] Assignment of Ref. (*65*) in agreement with optical spectra (*67*).

[e] Data from Ref. (*44*). The group *I4/mcm* has been assumed by analogy with $SrCrF_4$.

tem. Our *in-vacuo* calculations in CrF_6^{3-} give $\bar{\nu}(a_{1g})$ in the range 680–710 cm^{-1}, which means around 100–150 cm^{-1} over the experiment. Nevertheless, Barandiarán and Pueyo (*10*) found that the vibrational frequency $\bar{\nu}(a_{1g})$ of the U-SPDD calculation decreases about 150 cm^{-1} when the electrostatic potential of the K_2NaCrF_6 lattice is included in the SCF calculation. Since the structure of this lattice is identical to the one studied by Ferguson *et al.* (*31*) and Dubicki *et al.* (*32*), the discrepancies found between the *in-vacuo* calculations and the experimental values are within the range of the lattice effects expected.

From these comparisons we conclude that the *in-vacuo* calculations on the CrF_6^{n-} (n = 2–5) systems reported in this work give ground state R_e's and $\bar{\nu}(a_{1g})$s which deviate, at worst, 0.1–0.2 Å and 100–150 cm^{-1} from the observed values, respectively. In CrF_6^{4-} the predicted R_e's lie within the experimental range. These results are remarkably more consistent with the observations than the CNDO values in Ref. (*8*). Also, they have a quality comparable to that achieved, after inclusion of a certain type of cluster–lattice interaction, in Ref. (*11*). Furthermore, the nuclear potential for the CrF_6^{5-} ion shows a clear minimum in our best calculation, in contrast with the MS–$X\alpha$ results for $CuCl_6^{5-}$ in Ref. (*12*). The quality of the present calculation of R_e seems to be better than that appearing in analogous recent calculations. In relation with $\bar{\nu}(a_{1g})$, we recall that this quantity is often unknown for this type of compound. The excellent agreement reported in Ref. (*12*) (156 vs 160 cm^{-1} (observed)) for $\bar{\nu}(a_{1g})$ seems to be accidental, given the high sensitivity of this frequency to the functional representation of the nuclear potential. We can say that Richardson's methodology in the present form gives reasonably accurate values of $\bar{\nu}(a_{1g})$. Given the scarcity of the known data, these theoretical results are useful. Finally, the deviations from experiment obtained in these *in-vacuo* calculations are practically coincident with the shifts obtained by Barandiarán and Pueyo in K_2NaCrF_6 (*10*) when this methodology is augmented with a detailed (and expensive) treatment of the cluster–lattice interactions. This satisfactory result suggests that whereas the relatively economic *in-vacuo* calculation can give a faithful description of *families* of compounds with a common cluster unit, the rather expensive cluster-in-the-lattice calculation may be able to give very accurate predictions on the equilibrium geometry of a *particular* system of interest.

Acknowledgments

This work has been partially supported by the Comisión Asesora de Investigación Científica y Técnica (CAICYT), under Contract 2880/83. Two authors (EF, VL) are grateful for fellowships from the Ministerio de Educación y Ciencia.

References

1. P. Rabe and R. Haensel, *"Festkorperprobleme: Advances in Solid State Physics"* (J. Trensh, Ed.), Vol. 20, p. 43, Viewing, Braunschweig (1980).
2. M. Moreno, J. A. Aramburu, and M. T. Barriuso, *Phys. Lett. A* **87,** 307 (1982).
3. M. T. Barriuso and M. Moreno, *Phys. Rev. B: Condens. Matter* **26,** 2271 (1982).
4. M. T. Barriuso and M. Moreno, *Phys. Rev. B: Condens. Matter* **29,** 3623 (1984).
5. M. T. Barriuso and M. Moreno, *Solid State Commun.* **51,** 335 (1984).
6. M. T. Barriuso and M. Moreno, *Chem. Phys. Lett.* **112,** 165 (1984).
7. F. Rodríquez and M. Moreno, *J. Chem. Phys.* **84,** 692 (1986).
8. D. W. Clack, N. S. Hush, and J. R. Yandle, *J. Chem. Phys.* **57,** 3503 (1972).
9. L. Pueyo and J. W. Richardson, *J. Chem. Phys.* **67,** 3583 (1977).
10. Z. Barandiarán and L. Pueyo, *J. Chem. Phys.* **79,** 1926 (1983).

11. E. MIYOSHI AND H. KASHIWAGI, *Int. J. Quantum Chem.* **24,** 85 (1983).
12. H. CHERMETTE AND C. PEDRINI, *J. Chem. Phys.* **77,** 2460 (1982).
13. L. SEIJO, Z. BARANDIARÁN, V. LUAÑA, AND L. PUEYO, *J. Solid State Chem.* **61,** 269 (1986).
14. P. G. LYKOS AND R. G. PARR, *J. Chem. Phys.* **24,** 1166 (1956).
15. R. MCWEENY AND B. T. SUTCLIFFE, "Methods of Molecular Quantum Mechanics," Academic Press, Orlando/London (1969).
16. G. HÖJER AND J. CHUNG, *Int. J. Quantum Chem.* **14,** 623 (1978).
17. J. W. RICHARDSON, W. C. NIEUWPOORT, R. R. POWELL, AND W. F. EDGELL, *J. Chem. Phys.* **36,** 1057 (1962).
18. J. W. RICHARDSON, R. R. POWELL, AND W. C. NIEUWPOORT, *J. Chem. Phys.* **38,** 796 (1963).
19. R. E. WATSON, Tech. Rep. No. 12. M.I.T., Cambridge, Massachusetts (1959).
20. E. CLEMENTI AND C. ROETTI, *At. Data Nucl. Data Tables* **14,** 177 (1974).
21. S. GUTIÉRREZ ORELLANA AND L. PUEYO, *J. Solid State Chem.* **55,** 30 (1984).
22. L. SEIJO, thesis dissertation, Universidad de Oviedo (1983).
23. S. HUZINAGA AND A. A. CANTU, *J. Chem. Phys.* **55,** 5543 (1971).
24. V. LUAÑA AND L. PUEYO, *Quantum Chem.*, in press.
25. S. HUZINAGA AND M. YOSHIMINE, *J. Chem. Phys.* **68,** 4486 (1978).
26. O. GROPEN, S. HUZINAGA, AND A. D. MCLEAN, *J. Chem. Phys.* **73,** 402 (1980).
27. O. GROPEN, U. WAHLGREN, AND L. PETTERSSON, *Chem. Phys.* **66,** 453 and 459 (1982).
28. R. D. SHANNON AND C. T. PREWITT, *Acta Crystallogr. Sect. B* **25,** 925 (1969).
29. J. C. COUSSEINS AND A. DE KOZAK, *C.R. Acad. Sci. (Paris), Ser. C* **263,** 1533 (1966).
30. G. FERNÁNDEZ RODRIGO, L. PUEYO, M. MORENO, AND M. T. BARRIUSO, *J. Solid State Chem.*, in press.
31. J. FERGUSON, H. J. GUGGENHEIM, AND D. L. WOOD, *J. Chem. Phys.* **54,** 504 (1971).
32. L. DUBICKI, J. FERGUSON, AND B. VAN OOSTERHOUT, *J. Phys. C* **13,** 2971 (1980).
33. H. C. CLARK AND Y. N. SADANA, *Canad. J. Chem.* **42,** 50 (1964).
34. D. BABEL, "Structure and Bonding," Vol. 3, pp. 1–87, Springer-Verlag, New York/Berlin (1967).
35. G. SIEBERT AND R. HOPPE, *Z. Anorg. Allg. Chem.* **391,** 126 (1972).
36. H. BODE AND E. VOSS, *Z. Anorg. Allg. Chem.* **286,** 136 (1956).
37. G. SIEBERT AND R. HOPPE, *Z. Anorg. Allg. Chem.* **391,** 113 (1972); *Naturwissenschaften* **58,** 95 (1971).
38. K. KNOX, *Acta Crystallogr.* **13,** 507 (1960).
39. J. V. DEWAN AND A. J. EDWARDS, *J. Chem. Soc.* 533, (1977).
40. D. BABEL AND G. KNOKE, *Z. Anorg. Allg. Chem.* **442,** 151 (1978).
41. C. JACOBINI, R. DE PAPE, M. POULAIN, J. Y. LE MAROUILLE, AND D. GRANDJEAN, *Acta Crystallogr. Sect. B* **30,** 2688 (1974).
42. D. DUMORA, R. VAN DER MUHLL, AND J. RAVEZ, *Mater. Res. Bull.* **6,** 561 (1971).
43. K. K. WU AND I. D. BROWN, *Mater. Res. Bull.* **8,** 593 (1973).
44. D. DUMORA AND J. RAVEZ, *C.R. Acad. Sci. (Paris), Ser. C* **268,** 337 (1969).
45. A. DE KOZAK, *C.R. Acad. Sci. (Paris), Ser. C* **268,** 2184 (1969).
46. G. FÉREY, R. DE PAPE, M. POULAIN, D. GRANDJEAN, AND A. HARDY, *Acta Crystallogr. Sect. B* **33,** 1409 (1977).
47. K. KNOX AND D. W. MITCHELL, *J. Inorg. Nucl. Chem.* **21,** 253 (1961).
48. G. SIEVERT AND R. HOPPE, *Z. Anorg. Allg. Chem.* **391,** 117 (1972).
49. R. HAEGELE, W. VERSCHAREN, AND D. BABEL, *Z. Naturforsch. B* **30,** 462 (1975).
50. D. BABEL AND R. HAEGELE, *J. Solid State Chem.* **18,** 39 (1976).
51. J. ARNDT, D. BABEL, R. HAEGELE, AND N. ROMBACH, *Z. Anorg. Allg. Chem.* **418,** 193 (1975).
52. G. BRUNTON, *Mater. Res. Bull.* **4,** 621 (1969).
53. H. BODE AND E. VOSS, *Z. Anorg. Allg. Chem.* **290** 1 (1957); D. BABEL, G. PAUSEWANG, AND W. VIEBAHN, *Z. Naturforsch. B* **22,** 1219 (1967).
54. D. BABEL, *Z. Anorg. Allg. Chem.* **387,** 160 (1972).
55. W. VIEBAHN, *Z. Anorg. Allg. Chem.* **386,** 335 (1971).
56. D. BABEL, *Z. Anorg. Allg. Chem.* **406,** 23 (1974).
57. G. COURBION, C. JACOBINI, AND R. DE PAPE, *Acta Crystallogr. Sect. B* **33,** 1405 (1977).
58. J. CHASSAING, *C.R. Acad. Sci. (Paris), Ser. C* **268,** 2188 (1969).
59. M. VLASSE, J. P. CHAMINADE, J. M. DANCE, M. SAUX, AND P. HAGENMULLER, *J. Solid State Chem.* **41,** 272 (1982).
60. K. H. JACK AND R. MAITLAND, *Proc. Chem. Soc.* 232 (1957).
61. J. W. CABLE, M. K. WILKINSON, AND E. O. WOLLMAN, *Phys. Rev.* **118,** 950 (1960).
62. A. J. EDWARDS AND R. D. PEACOCK, *J. Chem. Soc.* 4126 (1959).
63. A. DE KOZAK, *Rev. Chim. Mineral.* **8,** 301 (1971).

64. D. BABEL, *Z. Anorg. Allg. Chem.* **336,** 200 (1965).
65. H. G. VON SCHNERING, B. KOLLOCH, AND A. KOLODZIEJCZYK, *Angew. Chem., Int. Ed. Eng.* **10,** 413 (1971).
66. R. VON DER MUHLL, D. DUMORA, J. P. RAVEZ, AND P. HAGENMULLER, *J. Solid State Chem.* **2,** 262 (1970).
67. D. DUMORA, C. FOUASSIER, R. VON DER MUHLL, J. P. RAVEZ, AND P. HAGENMULLER, *C.R. Acad. Sci. (Paris), Ser. C.* **273,** 247 (1971).